

# Aero-Optical Effects of Supersonic Boundary Layers

Stanislav Gordeyev\* and Eric Jumper†

University of Notre Dame, Notre Dame, Indiana 46556

and

Tim E. Hayden‡

U.S. Air Force Academy, Colorado Springs, Colorado 80840

DOI: 10.2514/1.J051266

**Aero-optical measurements of a zero-pressure-gradient, supersonic boundary layer along the test-section wall at  $M = 2.0$  were performed using a Malley probe. The Malley probe captured both the amplitude of optical distortions and the convective speed. The convective speed of the optically active structures inside the supersonic boundary layer was found to be 0.84 of the freestream speed. The deflection-angle spectra were found to collapse with the local displacement thickness. The streamwise correlation function for the supersonic boundary layer revealed the presence of a pseudoperiodic structure with the typical size of 1.5 of the local boundary-layer thickness. A new model was developed to describe aero-optical effects of both the subsonic and the supersonic boundary layers. Finally, this new model and several other theoretical scalings were tested in the attempt to collapse both subsonic and supersonic boundary-layer aero-optical results.**

## Nomenclature

|                    |   |
|--------------------|---|
| $A_p$              | = laser beam aperture                                       |
| $B$                | = constant, defined in Eq. (11)                             |
| $C$                | = function, defined in Eq. (12)                             |
| $C_f$              | = local skin friction                                       |
| $C_w$              | = constant, defined in Eq. (4a)                             |
| $c_p$              | = isobaric specific heat                                    |
| $F_1, F_2$         | = functions, defined in Eq. (11)                            |
| $f$                | = frequency   |
| $f(y/\delta)$      | = normalized mean velocity profile, used in Eq. (11)        |
| $G(A_p)$           | = aperture function   |
| $g(y/\delta)$      | = normalized fluctuating velocity profile, used in Eq. (11) |
| $K_{GD}$           | = Gladstone–Dale constant                                   |
| $M$                | = Mach number   |
| OPD                | = optical-path difference                                   |
| OPD <sub>rms</sub> | = root mean square of optical-path difference               |
| $p$                | = pressure  |
| $q$                | = dynamic pressure  |
| $Re_x$             | = Reynolds number based on $x$                              |
| $Re_{\Theta}$      | = Reynolds number based on $\Theta$                         |
| $r$                | = recovery factor   |
| $r_2$              | = function, defined in Eqs. (4b) and (4c)                   |
| $St$               | = Strouhal number   |
| $T$                | = temperature   |
| $t$                | = time  |
| $U$                | = time-averaged velocity component                          |
| $U_C$              | = mean convective speed                                     |
| $u$                | = fluctuating velocity component                            |
| $u_\tau$           | = skin-friction velocity                                    |
| $x, y$             | = coordinate system   |

|                 |   |
|-----------------|---|
| $\gamma$        | = heat-capacity ratio                                       |
| $\Delta$        | = difference  |
| $\delta$        | = boundary-layer thickness                                  |
| $\delta^*$      | = displacement boundary-layer thickness                     |
| $\Theta$        | = boundary-layer momentum thickness                         |
| $\theta$        | = deflection angle  |
| $\theta_{norm}$ | = normalized deflection-angle spectrum                      |
| $\Lambda_y$     | = wall-normal density correlation length                    |
| $\rho$          | = density   |
| $\rho_{SL}$     | = sea-level density, $1.225 \text{ kg} \cdot \text{m}^{-3}$ |
| $\rho_x$        | = streamwise autocorrelation function                       |

## Subscripts

|           |                                     |
|-----------|-------------------------------------|
| $\hat{f}$ | = Fourier transform of function $f$ |
| $i$       | = incompressible                    |
| rms       | = root-mean-squared value           |
| $w$       | = wall                              |
| 0         | = total                             |
| $\infty$  | = at infinity                       |

## I. Introduction

**L**ASER-BASED free-space communication systems offer high transmission rates through the atmosphere, on the order of terabytes per second. Once a link is established, high-speed, secure communication links between ground stations, aircraft, or satellites become possible; however, when the link involves aircraft, turbulent flow around the aircraft introduces density fluctuations, which can distort the emerging laser beam and significantly reduce laser intensity on a target [1,2]. These *aero-optical* effects increase significantly with Mach number and may cause the airborne free-space communication system to be inoperable at transonic and supersonic speeds.

Large-scale vortical structures inside shear layers and wakes behind bluff bodies introduce significant turbulent fluctuations and can impose large aero-optical distortions on the laser beam even at moderate subsonic speeds [3,4]. Attached turbulent boundary layers, although producing smaller density fluctuations compared with shear layers and wakes, have also shown to potentially create significant aero-optical distortions at high transonic and supersonic speeds [5,6].

Aero-optical distortions produced by subsonic boundary layers were extensively experimentally studied in the last 40 years [3,5–8]. Supersonic and hypersonic boundary layers, on the other hand, have been given significantly less attention, partially because of

Presented as Paper 2011-1325 at the 49th AIAA Aerospace Sciences Meeting and Exhibit, Orlando, FL, 4–7 January 2011; received 29 March 2011; revision received 18 July 2011; accepted for publication 4 September 2011. Copyright © 2011 by the authors. Published by the American Institute of Aeronautics and Astronautics, Inc., with permission. Copies of this paper may be made for personal or internal use, on condition that the copier pay the \$10.00 per-copy fee to the Copyright Clearance Center, Inc., 222 Rosewood Drive, Danvers, MA 01923; include the code 0001-1452/12 and \$10.00 in correspondence with the CCC.

\*Associate Research Professor, Department of Aerospace and Mechanical Engineering, Senior Member AIAA.

†Professor, Department of Aerospace and Mechanical Engineering, Fellow AIAA.

‡Aerospace Engineer, Department of Aeronautics, Senior Member AIAA.

experimental difficulties in making reliable optical measurements at high speeds. In 1956, Stine and Winovich [9] experimentally investigated the optical transmission characteristics of compressible turbulent boundary layers for the Mach number range from 0.4 to 2.5 by measuring the time-averaged intensity of light for flow-on cases compared with a flow-off case. They compared their experimental findings with the theoretical predictions of Liepmann [10] and found a reasonably good agreement. Later, these experimental results were further analyzed by Sutton [11], where he calculated length scales and provided a simple scaling for optical modulation transfer function to compute the level of optical degradation caused by compressible boundary layers for different flight regimes. Yanta et al. [12], reported measurements of aero-optical distortions by a flat-plate laminar boundary layer in a hypersonic facility at  $M = 7$ . They reported both near-field wave-front measurements and far-field intensities. Recently, Wyckham and Smits [8] reported results for hypersonic,  $M = 7.8$ , boundary-layer measurements with and without gas injection and reported estimates of correlation lengths.

This paper describes experimental measurements of optical distortions caused by supersonic boundary layers formed on the supersonic wind-tunnel walls. The experimental setup is described in Sec. II. Experimental results are presented in Sec. III. Several scaling predictions for levels of optical distortions caused by the boundary layers are compared and discussed. Finally, conclusions drawn from this work are summarized in Sec. IV.

## II. Experimental Setup

All aero-optical measurements were performed in the Trisonic Wind Tunnel at the U.S. Air Force Academy in Colorado Springs. The tunnel is an open-circuit, blowdown-type facility, with a range of Mach numbers between 0.24 and 4.5. The tunnel is shown schematically in Fig. 1, top. Air is passed through several stages of filters and dryers, and is compressed by two rotary screw compressors, 260 kW each to six 25 m<sup>3</sup> storage tanks at pressures up to 40 atmospheres. The stored air is heated to approximately 38°C to prevent complications due to water condensation and ice formation during high-Mach-number tests. The tunnel has a test section with a 0.3 × 0.3 m cross section with two 0.3 m round optical windows on both sides of the test section (see Fig. 1, bottom).

For all tests the freestream Mach number was 2.0; to change the test-section static density the plenum pressure was varied between 3.4 and 6.8 atmospheres, so the test-section static pressure was varied between 0.4 and 0.8 atmospheres. The results presented in this paper were obtained with a plenum pressure of 5.4 atmospheres. The static temperature was estimated to be between -107 and -109°C for different runs using the total temperature measurements and the isentropic relation.

All optical measurements were performed using a Malley probe [13]; the schematic of the experimental setup are shown in Fig. 2 and the optical bench can be seen in the foreground of Fig. 1, bottom. The laser beam, after passing through the spatial filter, was recollimated

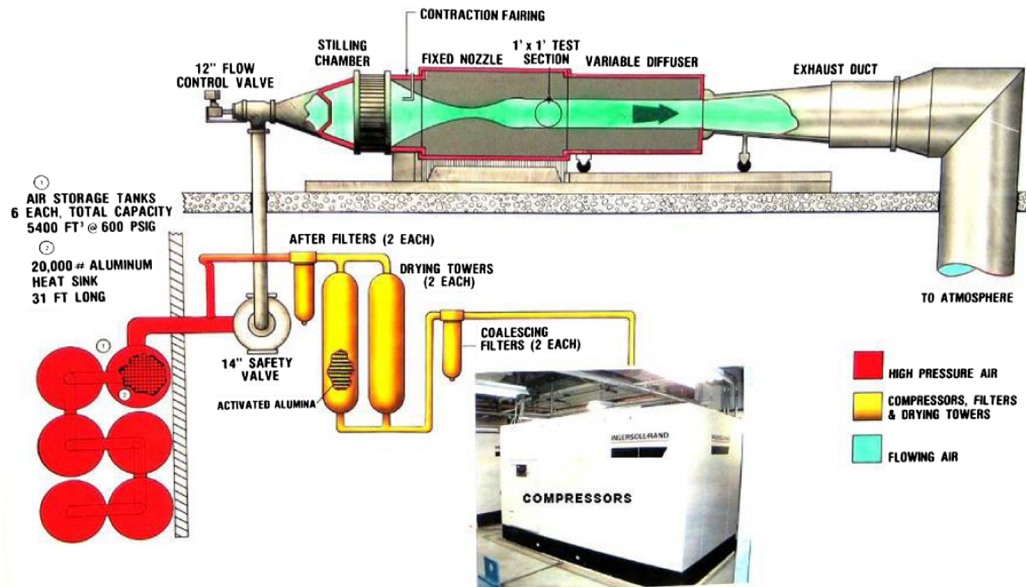


Fig. 1 Top: schematic of the U.S. Air Force Academy Trisonic Wind Tunnel. Bottom: the test section with 0.3-m-diam optical windows.

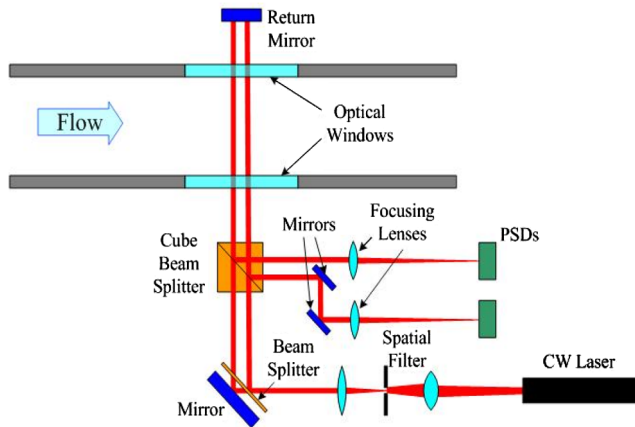


Fig. 2 Schematics of DBL experimental setup.

and split into two small (about a millimeter in diameter) parallel beams, separated in the streamwise direction by a known distance. The beam separation was varied between 6 and 11 mm for different runs. The beams were then forwarded into the test section normal to the optical window. The return mirror on the other side of the test section reflected beams back to the optical bench along the same optical path. The returning beams were split off using a cube beam splitter, and each beam was focused onto a position-sensing device (PSD), capable of measuring instantaneous beam deflections. The sampling frequency was 200 kHz and the sampling time was 10 s.

During the first test, the laser beams were passed into the empty test section, so they encountered two supersonic boundary layers, one on each side of the test section. This test is referred to as the double-boundary-layer (DBL) test. The beams' streamwise locations were varied to investigate the effect of the boundary-layer growth along the optical window.

During the second test, a wedge model was placed into the flow, with a mirror mounted flush on the zero-angle side of the wedge (see Fig. 3, left). Both beams were reflected from the small mirror back to the optical table exactly along the same optical path, then split to the PSD's as before. In this test the beams were traversed through only one boundary layer (and a weak Mach wave generated by the wedge); this test is referred to as the single-boundary-layer (SBL) test.

In addition to aero-optical tests, schlieren images of the wedge model (rotated 90 deg) in the test section were taken to visualize the flow pattern around it (see Fig. 3, right) and also to estimate the local boundary-layer thickness on the test-section wall, visible at the bottom of the schlieren image in Fig. 3 (right). The boundary layer at the center of the test-section window was found to be approximately 12 mm thick.

The Malley probe measures the instantaneous deflection angle,  $\theta(t)$ , which, assuming the frozen-flow hypothesis, is related to the

level of optical distortions,  $OPD(x)$ , as

$$\theta(t) = \frac{dOPD}{dx} = \frac{dx}{dt} \frac{dOPD}{dx} = -U_c \frac{dOPD}{dt}$$

where  $U_c$  is the convective speed of moving optical structures. Knowing the beam separation, the convective speed as a function of the frequency is also directly measured by the Malley probe by spectrally cross-correlating deflection angles of the two beams [13]. Finally, one-dimensional slices of  $OPD(t)$  can be calculated by integrating the deflection angle in time [13],

$$OPD(x = -U_c t) = -U_c \int_0^t \theta(t) dt \quad (1a)$$

or, equivalently, integrating the deflection-angle spectrum  $\hat{\theta}(f)$  in the Fourier domain:

$$OPD(x = -U_c t) = -U_c \cdot \int_{-\infty}^{\infty} \frac{\hat{\theta}(f) \cdot \exp(2\pi i f t)}{2\pi i f} df \quad (1b)$$

### III. Results

An example of the deflection-angle spectrum of the DBL tests at the aft portion of the optical window is shown in Fig. 4, top; the phase or the argument of the spectral cross-correlation function between two beams is shown in Fig. 4, bottom. Sharp peaks at low frequencies below 3 kHz are tunnel-related vibration peaks; also some amount of contamination was observed between 3 and 10 kHz. Peaks at 25, 54, and 70 kHz are electronic noise from PSD conditioning units. The wide hump centered around 25 kHz in the deflection-angle spectrum is due to the supersonic boundary layer. The optically active structures between 10 and 100 kHz convect at a constant speed of approximately 437 m/s, or 0.84 of the freestream speed, thus justifying the frozen-field hypothesis for this frequency range. Analysis of the convective speeds at all measurement locations over the window gave the average normalized convective speed of  $0.84 \pm 0.02$ . Although within experimental error, this value is slightly higher than the value of 0.82 of the freestream speed observed for subsonic boundary layers [6], later in this paper this slight increase in the convective speed at high Mach numbers will be shown to be consistent with theoretical considerations.

As it was already mentioned, the deflection-angle spectra were sampled at 200 kHz, so no information about aero-optical structures above 100 kHz is available. Also, the Malley probe beams were approximately 1 mm in diameter and any information about structures at scales less than the beam diameter is lost due to spatial averaging. Although this high-frequency, above 100 kHz, range might provide some information about aero-optical structures at small scales, Eq. (1b) shows that in order to calculate OPD, the deflection-angle spectrum should be divided by  $2\pi f$ ; thus, the

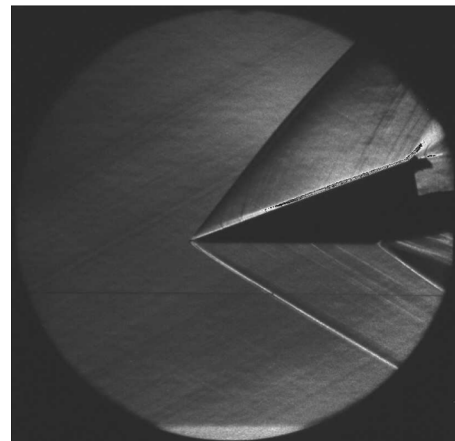
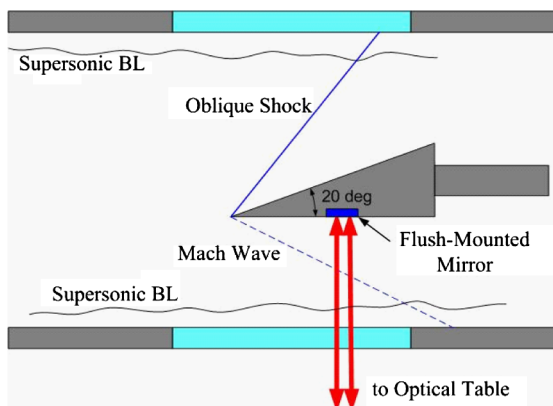


Fig. 3 Left: schematic of SBL experimental setup. Right: the schlieren picture of the flow around the wedge. The boundary layer is visible at the bottom of the optical window.

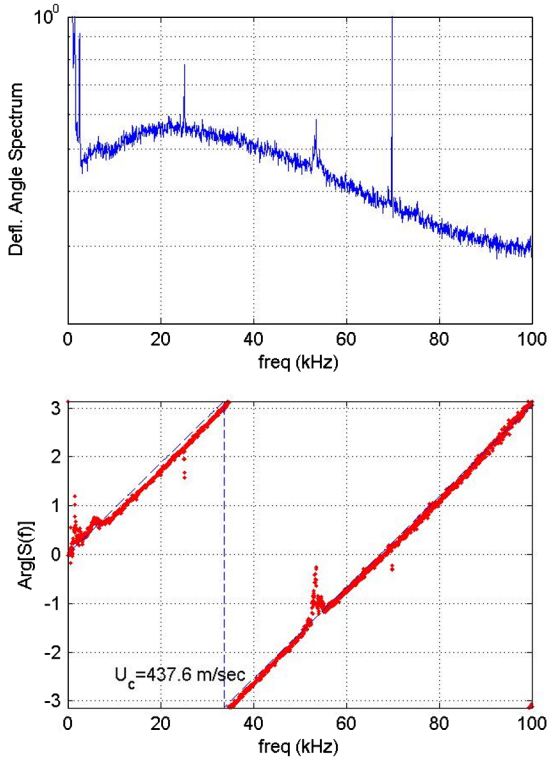


Fig. 4 Top: deflection-angle spectrum. Bottom: the phase between two laser beams (dots) and a linear fit (dashed line) with a corresponding convective speed. Beams were located 28 cm from the beginning of the optical window, beam separation was 6.5 mm.

overall OPD-contribution from high-frequency components is small compared with the contribution from the low-frequency range.

A. Scaling with the Boundary-Layer Thickness

Raw deflection-angle spectra at different window locations for both the DBL and SBL are presented in Fig. 5 (left). The DBL spectra were first divided by 2 to account for a double pass and then divided by  $\sqrt{2}$  to obtain spectra due to a single boundary layer [5]. The location of the hump is a function of the streamwise location, with the hump location around 25 kHz in the front of the optical window and shifting to a lower frequency of 22 kHz at the most downstream location on the optical window. Also, the amplitude of the hump increases downstream. All of these observations are consistent with the supersonic boundary layer growing downstream along the test section. Similar to the scaling arguments for subsonic boundary layers [5,6,14], the amplitude of optical distortions is proportional to the boundary-layer thickness and the location of the hump is inversely proportional to the boundary-layer thickness.

In [14] it was shown that subsonic boundary-layer deflection-angle spectra  $\hat{\theta}(f)$  scale with the freestream conditions and the local boundary-layer displacement thickness as

$$\hat{\theta}(f) \sim F(M) \frac{\rho_\infty}{\rho_{SL}} \delta^* \frac{1}{U_c} \hat{\theta}_{norm}(St_{\delta^*}) \quad (2)$$

where  $St_{\delta^*} = f\delta^*/U_\infty$  is the Strouhal number;  $\rho_\infty$  and  $U_\infty$  are the freestream density and the speed, respectively;  $\rho_{SL} = 1.225 \text{ kg/m}^3$  is the sea-level density;

$$\delta^* = \int_0^\infty \left(1 - \frac{\rho(y)U(y)}{\rho_\infty U_\infty}\right) dy$$

is the compressible displacement thickness; and  $U_c = 0.84U_\infty$  is the convective speed of the optical distortions. For subsonic speeds the Mach-dependent function  $F(M)$  was found to be  $F(M) = M^2$ ; the Mach scaling for supersonic speeds will be discussed later in this paper.

From schlieren pictures of the flow (see Fig. 3, right), the boundary-layer thickness,  $\delta$ , was estimated to be approximately 12 mm in the middle of the test section. From Fig. 6 (left), the ratio between the boundary-layer (BL) thickness and the displacement thickness at  $M = 2$  was estimated as  $\delta/\delta^* = 4.37$ , giving the absolute value of the displacement thickness near the middle of the optical window as  $\delta^*(x = 10 \text{ cm}) = 2.75 \text{ mm}$ . The displacement thicknesses at other locations of the optical windows were varied to collapse all measured deflection-angle spectra onto one curve. Results of the normalized deflection-angle spectra are shown in Fig. 5 (right). All curves were successfully collapsed over the wide range of frequencies, except for low frequencies below 10 kHz; as discussed earlier, this range of frequencies is corrupted by tunnel vibrations. The location of the normalized peak was found to be at approximately  $f_{peak}\delta^*/U_\infty = 0.13$ , which is very close to the peak value of 0.14 reported for subsonic boundary layers [5,6].

Based on the experimentally obtained displacement thicknesses, a corresponding boundary-layer growth,  $\delta(x)$ , is plotted in Fig. 6 (right) over the optical window. The boundary layer was found to grow by approximately 25% across the optical window; the results agree well with simple incompressible boundary-layer growth estimations, also presented in Fig. 6 (right). The approximate validity of these estimations for the compressible boundary layer was experimentally confirmed [15], as the boundary-layer thickness (unlike the displacement and the momentum thicknesses) does not depend on the Mach number, but only on the local  $Re_x$ . The virtual boundary-layer origin was found to be approximately 1 m upstream of the front of the optical window; this value corresponds well with the location of the nozzle throat, which is 1 m upstream of the optical window. Based on this virtual origin value, the Reynolds number over the optical window was found to be approximately  $Re_x = 70 \times 10^6$ .

The final important remark is that, as shown in Fig. 6 (right), just by scaling boundary-layer deflection-angle spectra, the Malley probe was able to *nonintrusively* measure the thickness of the boundary

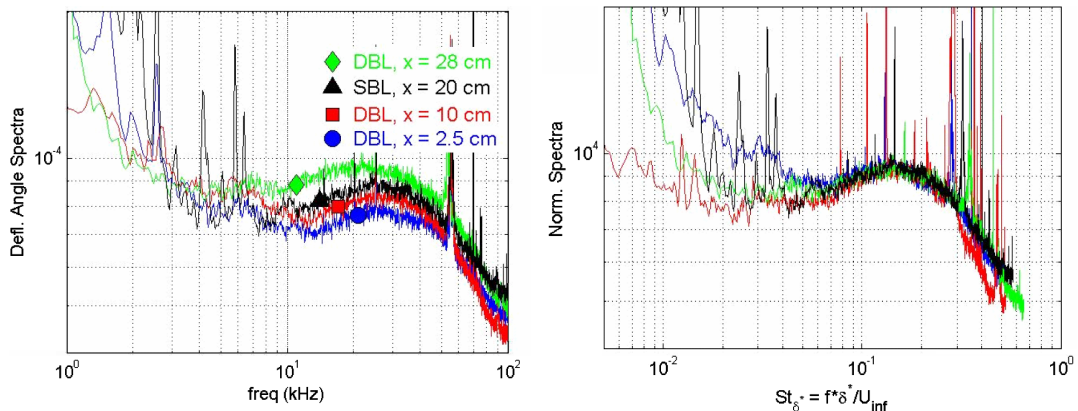


Fig. 5 Raw (left) deflection-angle spectra and normalized (right) spectra as defined in Eq. (2) at different locations over the optical window.

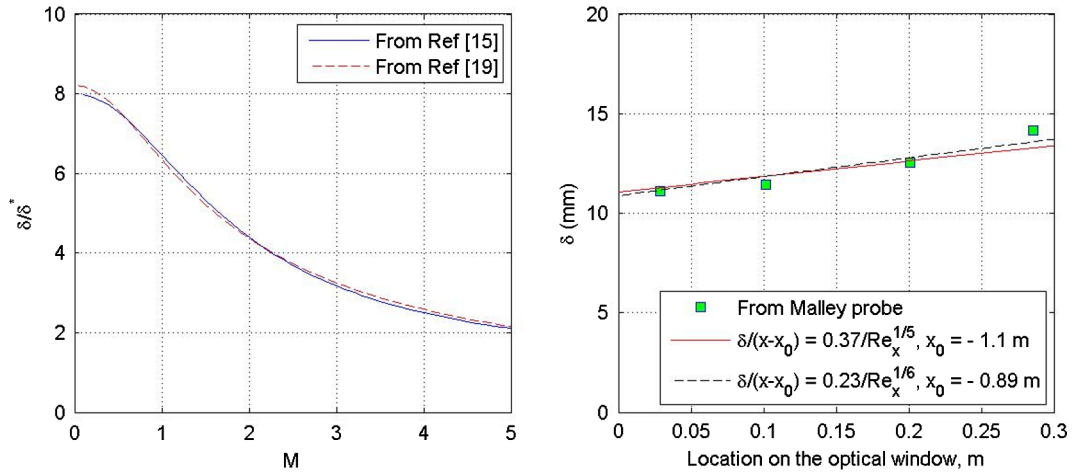


Fig. 6 Left:  $\delta/\delta^*$  as a function of freestream Mach number. Right: boundary-layer growth over the optical window: experimental measurements using the Malley probe and the turbulent-boundary-layer growth estimation.

layer along the test section by propagating small-aperture laser beams through and normal to the boundary layer.

### B. Scaling with Mach Number

Optical measurements in wind tunnels at high speeds are usually complicated by tunnel mechanical vibrations, which easily corrupt optical measurements when using conventional wave-front sensors, like Shack–Hartmann and distorted-grating sensors [8,16]. The Malley probe identifies frequencies with potential vibration-related corruption and an estimate of the physically related aero-optical spectrum is available. Another advantage of the Malley probe is high temporal resolution and long sampling times, which, assuming frozen flow, provide 1-D slices of wave fronts with high spatial and temporal resolution over reasonably large apertures. Finally, the spectra-matching method, described in [14], which compares deflection-angle spectra measured by the Malley probe, provides correct levels of aero-optical distortion even in high-vibrational environments.

In the previous section it was shown that supersonic boundary-layer optical spectra collapse onto one curve when normalized by

$$\frac{\rho_\infty}{\rho_{SL}} \delta^* \frac{1}{U_c}$$

similar to the subsonic optical spectra. Several models have been developed to predict the Mach dependence. In [5] the following model for the optical distortions in a subsonic boundary layer for adiabatic and heated walls was proposed and experimentally verified for  $M < 0.6$  over a range of heated/cooled walls:

$$OPD_{rms} = 1.7 \times 10^{-5} G(\text{Ap}) \frac{\rho_\infty}{\rho_{SL}} \delta^* \left( M^2 + 2.2 \frac{\Delta T}{T_\infty} \right) \quad (3)$$

where  $\Delta T = T_w - T_r$  is the difference between the wall temperature  $T_w$  and the recovery temperature  $T_r$ ,  $G(\text{Ap})$  is an aperture function [6], and  $\rho_{SL}$  is the sea-level density ( $1.225 \text{ kg/m}^3$ ).

Wyckham and Smits [8] proposed the following model:

$$OPD_{rms} = C_w K_{GD} \rho_\infty \delta M_\infty^2 \sqrt{C_f r_2^{-3/2}} \quad (4a)$$

where  $K_{GD}$  is a Gladstone–Dale constant ( $K_{GD} = 2.27 \times 10^{-4} \text{ m}^3/\text{kg}$  in the visible-light range), and for adiabatic walls,

$$r_2 = 1 + \frac{\gamma - 1}{2} M_\infty^2 [1 - r(U_c/U_\infty)^2] \quad (4b)$$

or, for heated or cooled walls,

$$r_2 = 0.5(T_w/T_\infty + 1) \quad (4c)$$

where  $r$  is the recovery factor. Experimentally, they found  $C_w$  to be between 0.7 and 1.0 for a range of Mach numbers between 0.8 and 7.8.

Finally, Rose [7] empirically found that the optical distortions are proportional to the dynamic pressure and the boundary-layer thickness for subsonic speeds:

$$OPD_{rms} \sim q \delta, \quad q = p_0 - p \quad (5)$$

To check all these theories, the boundary-layer deflection-angle spectrum at the optical window location of  $x = 10$  cm was compared with the deflection-angle spectrum for the adiabatic subsonic,  $M = 0.6$ , boundary layer. Details about the subsonic boundary-layer measurements can be found in [5].

Table 1 presents parameters for the supersonic boundary layer and for the subsonic data of [6]. The velocity profile of the subsonic boundary layer was measured using hot wire and the various boundary-layer thicknesses and the local skin-friction coefficient was calculated from it. For the supersonic boundary layer, the incompressible skin-friction coefficient  $C_{f,i}$  was calculated from the local Reynolds number using the von Kármán–Schoenherr correlation [17]:

$$C_{f,i} = \frac{1}{17.08(\log_{10} Re_\Theta)^2 + 25.11 \cdot \log_{10} Re_\Theta + 6.012}$$

For the  $M = 2.0$  case, the boundary-layer momentum thickness,  $\Theta$ , was estimated to be  $\Theta = 0.083\delta$ , [15], thus giving  $Re_\Theta = 69,000$ . The compressible skin friction  $C_f$  was found by applying a compressible correction [18,19],  $C_f/C_{f,i} = 0.76$  for  $M = 2.0$ .

From Eqs. (1a) and (1b), it can be shown that the deflection-angle spectrum should scale as

$$\hat{\theta}(f) \sim (OPD_{rms}/U_c) \hat{\theta}_{norm}(St_{\delta^*})$$

The normalized deflection-angle spectra for both the subsonic and the supersonic cases were calculated for each theoretical prediction,

Table 1 Boundary-layer parameters

| Case          | $\delta$ , mm | $\delta^*$ , mm | $Re_x$           | $Re_\Theta$ | $C_f$                 | $q$ , Pa          | $U_\infty$ , m/s | $\rho_\infty$ , kg/m <sup>3</sup> |
|---------------|---------------|-----------------|------------------|-------------|-----------------------|-------------------|------------------|-----------------------------------|
| BL, $M = 0.6$ | 25            | 3.6             | $19 \times 10^6$ | 27,000      | $2.0 \times 10^{-3}$  | $2.1 \times 10^4$ | 204              | 1.0                               |
| BL, $M = 2.0$ | 12            | 2.75            | $70 \times 10^6$ | 69,000      | $1.44 \times 10^{-3}$ | $5.8 \times 10^5$ | 514              | 1.4                               |

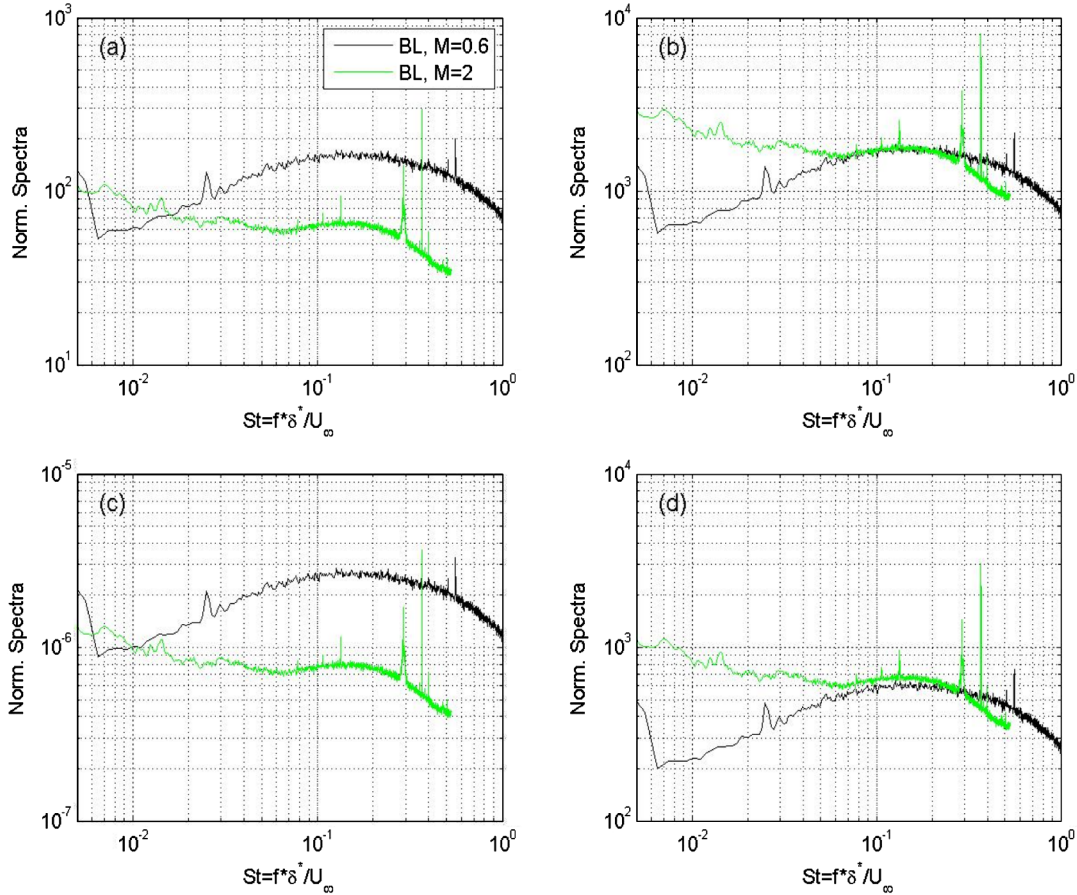


Fig. 7 Scaled subsonic and supersonic boundary-layer optical spectra using a) Eq. (3), b) Eqs. (4a) and (4b), c) Eq. (5), and d) Eq. (11).

assuming an adiabatic wall; the results are presented in Fig. 7. Neither scaling equation (3) nor Eq. (5) collapse the experimental data, whereas scaling equations (4a), (4b), and (11) provide a reasonable collapse. The  $\rho M^2$  scaling (3) was derived for subsonic flows only assuming weak compressibility and therefore was not expected to work at supersonic speeds. This model was modified to include strong compressibility effects at high Mach numbers [see Eq. (11)]. The full model derivation is presented later in this paper. The dynamic-pressure scaling (5) also failed to properly scale the data, because the OPD should be proportional to the freestream density, whereas the dynamic pressure is proportional to the freestream pressure, which is the product of the freestream density *and* the temperature. Therefore, OPD cannot be just proportional to  $q$  due to dimensional requirements.

The test-section walls were at approximately  $T_w = 21^\circ\text{C} = 294\text{ K}$ , and the freestream flow was  $T_\infty = -107^\circ\text{C} = 166\text{ K}$ . Since the tunnel run times were shorter than 30 s, it was not long enough to bring the test-section walls to thermal equilibrium with the flow; thus, the boundary layer for the supersonic-flow case developed over a slightly heated wall. To estimate the possible heating effect on the aero-optical boundary-layer performance, a subsonic approximation for a heated-wall boundary layer was used [Eq. (3)]:

$$\text{OPD}_{\text{rms}} \sim (M_\infty^2 + 2.2 \cdot (T_w - T_r)/T_\infty)$$

The recovery temperature can be estimated as

$$T_r = T_\infty(1 + r(\gamma - 1)/2M^2) = 288\text{ K}$$

giving  $2.2 \cdot (T_w - T_r)/T_\infty \sim 0.08$ . This term is much smaller than the  $M^2$  term, so wall-temperature effects can be ignored for this supersonic boundary layer.

### C. Aero-Optical Boundary-Layer Structure

From Fig. 7b, it can be observed that the normalized subsonic and supersonic spectra are nearly identical in the range of normalized frequencies,  $f\delta^*/U_\infty$ , between 0.06 and 0.3. For frequencies  $f\delta^*/U_\infty < 0.06$ , or, in dimensional units,  $f < 10\text{ kHz}$ , the aero-optical spectrum of the supersonic boundary layer is most probably corrupted by tunnel vibrations, as the phase in this range deviates from the expected straight line (see Fig. 4, bottom curve). For high frequencies above  $f\delta^*/U_\infty > 0.3$ , the supersonic boundary-layer aero-optical spectrum is consistently below the subsonic boundary-layer spectrum. This frequency range corresponds to aero-optical structures with wavelengths  $\Lambda$  smaller than

$$\Lambda_{\text{high}} = \delta^*(U_c/U_\infty)/0.3 = 2.8\delta^* = 7.7\text{ mm}$$

Thus, these small-scale structures are less optically active than the similar small-scale structures in the subsonic boundary layer.

Knowing the deflection-angle time history and the local convective speed, one-dimensional slices of OPD over an infinitely large aperture can be calculated using Eq. (1a). Before applying the integration, the deflection-angle signal was high-pass-filtered above 10 kHz to eliminate various sources of the contamination at low frequencies, discussed earlier. wave fronts then can be cut into smaller apertures and, after removing the piston and the tilt, the resulting  $\text{OPD}_{\text{rms}}$  can be calculated as a function of the aperture. Results normalized by the infinite-aperture  $\text{OPD}_{\text{rms}}$  are presented in Fig. 8 (left), along with the results for the  $M = 0.6$  subsonic boundary layer [6]. For both cases, it takes about 10 boundary-layer thicknesses to include all relevant optical distortions, implying that optically active large-scale boundary-layer structures are several boundary-layer thicknesses long.

To further investigate the difference between optical structures for the subsonic boundary layer [6] and the supersonic boundary layer, the correlation function of the wave front,

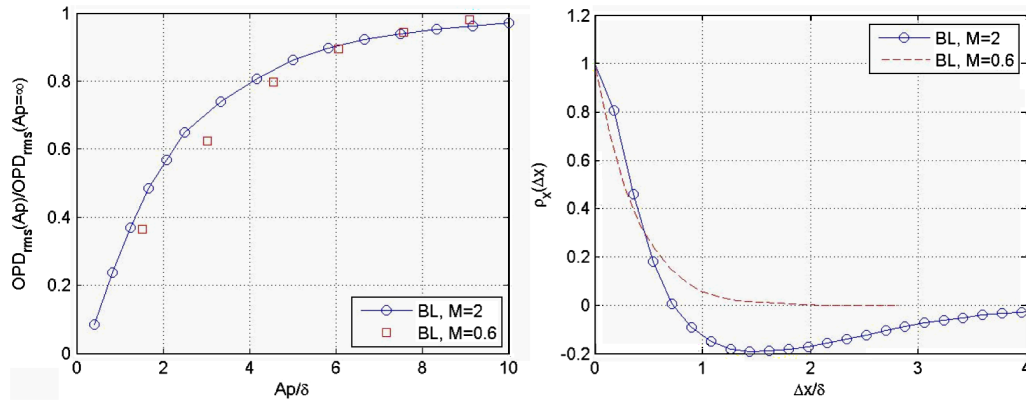


Fig. 8 Left: tip-removed aperture  $OPS_{rms}$  normalized by the infinite-aperture  $OPS_{rms}$  as a function of the aperture for the supersonic and subsonic boundary layers. Right: normalized correlation OPD as a function of the streamwise separation for the supersonic and subsonic boundary layers.

$$\rho_x(\Delta x = -U_C \Delta t) = \langle OPD(t)OPD(t + \Delta t) \rangle$$

was calculated for the aperture  $Ap = 10\delta$ ; the results are presented in Fig. 8 (right). Whereas the subsonic boundary-layer correlation function is monotonic and positive for all streamwise separations, the supersonic BL correlation function has a local minima at  $\Delta x/\delta = 1.5$ , implying pseudoperiodic aero-optical structures in the streamwise direction. Note that the frequency-peak location in Fig. 5 (right) is approximately  $f_{peak}\delta^*/U_\infty = 0.13$ , assuming that the underlying dominant aero-optical structure has a wavelength of  $\Lambda_{peak} = U_C/f_{peak}$ , or

$$\frac{\Lambda_{peak}}{\delta} = \frac{1}{0.13} \frac{\delta^*}{\delta} \left( \frac{U_C}{U_\infty} \right) = 1.5$$

which is the same as the location of the first minima in Fig. 8 (right). A similar correlation length of  $1.2\delta$  was observed in the transonic,  $M = 0.78$ , boundary layer [8].

#### D. Model for Aero-Optical Distortions for Supersonic Boundary Layers

As discussed above, the model equation (3), although correctly predicting aero-optical aberrations of the subsonic boundary layer with heated and cooled walls [5,6], does not take into account changes of the mean density and temperature profiles across the boundary layer and overpredicts the level of aero-optical distortions for the supersonic boundary layer. Let us revisit the model derivation in an attempt to improve its predictions for a large range of Mach numbers. For simplicity, we will derive the modified model for adiabatic walls only, although effects of heated/cooled walls can be incorporated, similar to how it was done for the model equation (3) [5].

The Walz equation or modified Crocco–Busemann relations (sometimes also called the “extended” strong Reynolds analogy) [15] for adiabatic walls is

$$c_p T'' = -r\tilde{u}u'' \quad (6)$$

where  $c_p$  is the constant pressure specific heat,  $\tilde{u}$  is the Favre-averaged mean velocity, and  $T''$  and  $u''$  are the Favre-averaged fluctuating temperature and velocity, respectively. The Favre-averaging can be replaced with the Reynolds-averaging, since they differ less than 1.5% for Mach numbers less than 3 [15]:

$$c_p T' = -r\bar{U}u' \quad (7)$$

From the equation of state  $P = \rho RT$ , the density fluctuations can be estimated from temperature fluctuations, assuming the static pressure is constant across the boundary layer:

$$\begin{aligned} \frac{\rho_{rms}(y)}{\rho(y)} &= -\frac{T_{rms}(y)}{T(y)}, \rightarrow \rho_{rms}(y) = -T_{rms}(y) \frac{\rho_\infty}{T_\infty} \frac{\rho(y)/\rho_\infty}{T(y)/T_\infty} \\ &= -T_{rms}(y) \frac{\rho_\infty}{T_\infty} \frac{1}{(T(y)/T_\infty)^2} \end{aligned} \quad (8)$$

Using the Morkovin scaling [20],

$$\sqrt{\frac{\rho(y)}{\rho_w} \frac{u_{rms}(y)}{u_\tau}} = g(y/\delta)$$

where  $u_\tau$  is the skin-friction velocity and  $\rho_w$  is the density near the wall, assuming the self-similarity of the mean velocity profile,  $U(y)/U_\infty = f(y/\delta)$ , and substituting both approximations into Eqs. (7) and (8), we get the following expression for density fluctuations across the boundary layer:

$$\begin{aligned} \rho_{rms}(y) &= \rho_\infty \frac{rU_\infty f(y/\delta) u_\tau \sqrt{\rho_w/\rho(y)} g(y/\delta)}{c_p T_\infty (T(y)/T_\infty)^2} \\ &= \rho_\infty \frac{(\gamma - 1) r U_\infty f(y/\delta) U_\infty \sqrt{C_f/2} \sqrt{T(y)/T_0} g(y/\delta)}{a_\infty^2 (T(y)/T_\infty)^2} \\ &= \rho_\infty \frac{(\gamma - 1) r M_\infty^2 \sqrt{C_f/2} f(y/\delta) \sqrt{T(y)/T_0} g(y/\delta)}{(T(y)/T_\infty)^2} \\ &= \rho_\infty \frac{(\gamma - 1) r M_\infty^2 \sqrt{C_f/2} \sqrt{T_\infty/T_0} f(y/\delta) g(y/\delta)}{(T(y)/T_\infty)^{3/2}} \end{aligned} \quad (9)$$

Using the adiabatic relation between the static temperature and the velocity, Eq. (9) can be finally written as

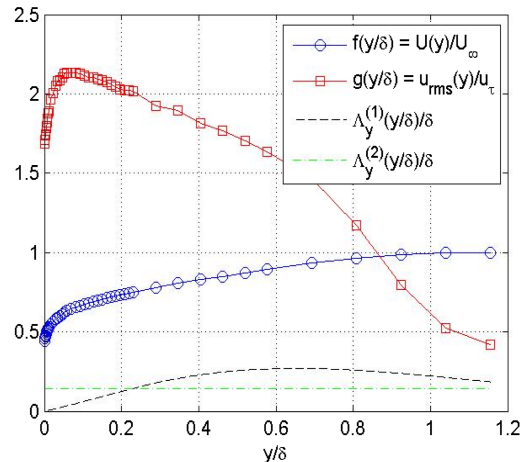
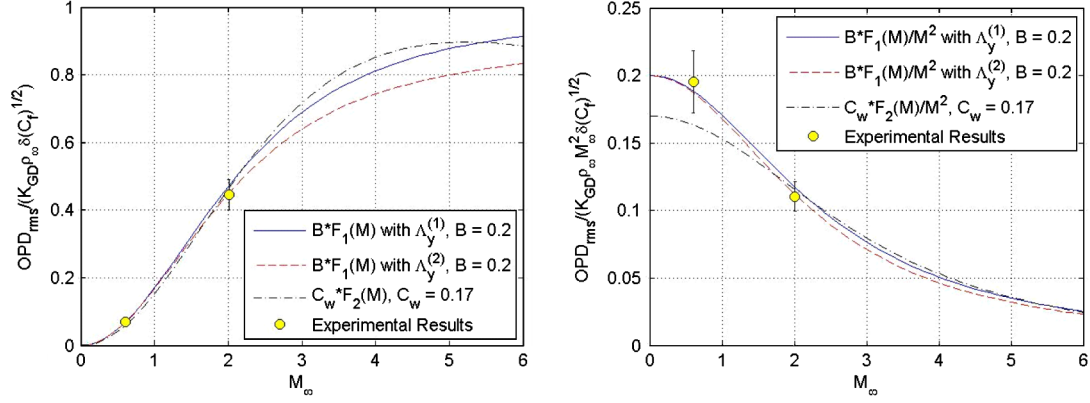


Fig. 9 Normalized mean and fluctuation velocity profiles and the two tested density correlation functions (from [22,23]).



**Fig. 10** Comparison between theoretical predictions, Eqs. (4a), (4b), and (11), and experimental data:  $OPD_{rms}/(K_{GD}\rho_{\infty}\delta(C_f)^{1/2})$  (left) and  $OPD_{rms}/(K_{GD}\rho_{\infty}M_{\infty}^2\delta(C_f)^{1/2})$  (right) as a function of Mach number.

$$\rho_{rms}(y) = \rho_{\infty}(\gamma - 1)rM_{\infty}^2\sqrt{C_f/2}\left(1 + \frac{(\gamma - 1)}{2}M_{\infty}^2\right)^{-1/2} \times \frac{f(y/\delta)g(y/\delta)}{\left(1 + \frac{(\gamma - 1)}{2}M_{\infty}^2[1 - f^2(y/\delta)]\right)^{3/2}} \quad (10)$$

To estimate the level of optical distortions by boundary layers, the estimated density fluctuations are substituted into the linking equation [21] to get the following equation for  $OPD_{rms}$ :

$$OPD_{rms} = \sqrt{2}K_{GD}\rho_{\infty}\delta(\gamma - 1)rM_{\infty}^2\sqrt{C_f/2}\left(1 + \frac{(\gamma - 1)}{2}M_{\infty}^2\right)^{-1/2} \times \left(\int_0^{\infty} \left[\frac{f(y/\delta)g(y/\delta)}{\left(1 + \frac{(\gamma - 1)}{2}M_{\infty}^2[1 - f^2(y/\delta)]\right)^{3/2}}\right]^2 \frac{\Lambda_y(y/\delta)}{\delta} d(y/\delta)\right)^{1/2}$$

or  $OPD_{rms} = C(0)K_{GD}\rho_{\infty}M_{\infty}^2\delta\sqrt{C_f}\frac{C(M_{\infty})}{C(0)}$

$$= BK_{GD}\rho_{\infty}\delta\sqrt{C_f}F_1(M_{\infty}) \quad (11)$$

where

$$C(M_{\infty}) = (\gamma - 1)r\left(1 + \frac{(\gamma - 1)}{2}M_{\infty}^2\right)^{-1/2} \times \left(\int_0^{\infty} \left[\frac{f(y/\delta)g(y/\delta)}{\left(1 + \frac{(\gamma - 1)}{2}M_{\infty}^2[1 - f^2(y/\delta)]\right)^{3/2}}\right]^2 \frac{\Lambda_y(y/\delta)}{\delta} d(y/\delta)\right)^{1/2} \quad (12)$$

$B = C(0)$ ,  $F_1(M_{\infty}) = M_{\infty}^2 C(M_{\infty})/C(0)$ , and  $\Lambda_y(y/\delta)$  is a wall-normal density correlations length; two different correlation lengths were used to estimate  $OPD_{rms}$ ,  $\Lambda_y^{(1)}(y/\delta)$  is provided by Gilbert [22] and  $\Lambda_y^{(2)}(y/\delta)$  is measured by Rose and Johnson [23].

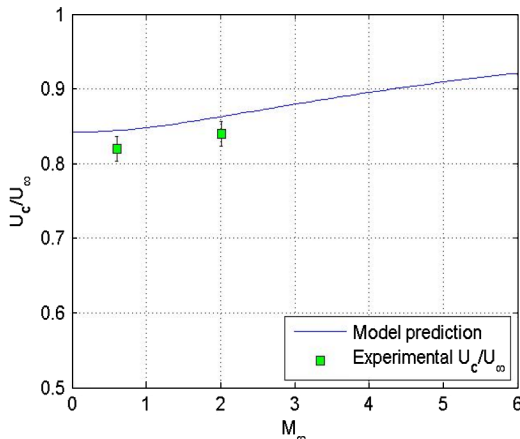


**Fig. 11** Model-calculated optical-structure convective speeds and experimental results.

Note that both the model (11) and the model (4a) and (4b) have the same functional form,  $OPD_{rms} \sim K_{GD}\rho_{\infty}\delta\sqrt{C_f}$ , but a different Mach-number-dependent function,  $F_1(M_{\infty})$  for the modified model equation (11) and

$$F_2(M_{\infty}) = M_{\infty}^2\left(1 + \frac{\gamma - 1}{2}M_{\infty}^2\left[1 - r\left(\frac{U_c}{U_{\infty}}\right)^2\right]\right)^{-3/2}$$

for the model equation (4a) and (4b). To calculate  $F_1(M_{\infty})$  from Eq. (12), experimentally measured velocity profiles for a  $M = 0.5$  boundary layer were used; Fig. 9 shows the wall-normal variation of  $f(y/\delta)$ ,  $g(y/\delta)$ ,  $\Lambda_y^{(1)}(y/\delta)$ , and  $\Lambda_y^{(2)}(y/\delta)$ .

To compare predictions from both models over the range of Mach numbers, constants  $B$  and  $C_w$  were adjusted to best match the experimental data for  $M = 0.6$  and  $2.0$  boundary layers: functions  $B \cdot F_1(M_{\infty})$ , with  $B = 0.20$  for two different correlation length functions,  $\Lambda_y^{(1)}(y/\delta)$  and  $\Lambda_y^{(2)}(y/\delta)$ , and  $C_w \cdot F_2(M_{\infty})$ , with  $C_w = 0.17$ , are plotted in Fig. 10, along with properly scaled experimental data. Note that the value of  $C_w$  is smaller than it was reported in [8]. The model equation (11) shows some dependence on the chosen correlation length function, as  $B \cdot F_1(M_{\infty})$  with  $\Lambda_y^{(1)}(y/\delta)$  is consistently above  $B \cdot F_1(M_{\infty})$  with  $\Lambda_y^{(2)}(y/\delta)$ , as the density correlation lengths  $\Lambda_y^{(2)}(y/\delta)$  are smaller than  $\Lambda_y^{(1)}(y/\delta)$ ; note that this difference can be somewhat minimized by adjusting the constant  $B$  for each function. Both models (11), (4a), and (4b) agree fairly well over a range of supersonic Mach numbers between 1 and 6; the model (4a) and (4b) underpredicts the level of optical aberration for the subsonic boundary layer by 10–15% for subsonic Mach numbers from 0 to 1. Numerical integration of Eq. (12) gives the value of  $B_{theory} = 0.22$  using  $\Lambda_y^{(1)}(y/\delta)$ , and the value of  $B_{theory} = 0.19$  using  $\Lambda_y^{(2)}(y/\delta)$ ; these values are close to the experimental value of  $B = 0.20$ .

As a final remark, since the optical aberrations are related to density fluctuations, the optical-structure convective speed can be estimated by using a weighted integral, with  $\rho_{rms}(y)$  as a weighting function:

$$U_c = \int_0^{\infty} \rho_{rms}(y)U(y) dy / \int_0^{\infty} \rho_{rms}(y) dy$$

Calculations of the convective speed as a function of the freestream Mach number are presented in Fig. 11; also in the same figure, experimentally measured convective speeds for  $M = 0.6$  and  $2.0$  boundary layers are presented for comparison. Although the modified model slightly overpredicts the absolute value of the convective speed, it does correctly predict the experimentally observed increase of the convective speed with the Mach number.

## IV. Conclusions

The experimental measurements of aero-optical distortions of the  $M = 2.0$  supersonic boundary layer on the wind-tunnel wall using

the Malley probe are presented. The deflection-angle spectra were measured at different locations over the optical window for different freestream densities. It was shown that the spectra collapse onto one curve when normalized by the boundary-layer displacement thickness and the freestream density. The mean convective speed of the optically active structures was measured as 0.84 of the freestream speed, which is slightly larger than the convective speed of 0.82 of the optical structures observed for subsonic boundary layers. The boundary-layer thickness variation over the optical window was nonintrusively measured by the Malley probe.

Several scalings were tested to see whether they collapse aero-optical results for both the subsonic and the supersonic boundary layers. Two models, the model equation (4a) and the new model equation (11) presented in this paper, were found to reasonably predict levels of the aero-optical aberrations caused by boundary layers for both subsonic and supersonic Mach numbers. Note that in order to match experimental data presented in this paper, the constant in the model equation (4a) had to be adjusted to a smaller value than was reported earlier.

The small-scale structures in the  $M = 2.0$  supersonic boundary layer were found to be less optically active, compared with the subsonic boundary layer. From the streamwise correlation measurements it was found that the dominant optical structure in the supersonic boundary layer is weakly periodic, with the typical length of 1.5 of the boundary-layer thickness. The minimum aperture size was found to be at least 10 boundary-layer thicknesses to include all aero-optical effects from the boundary layer; a similar aperture size was observed for the subsonic boundary layer. Smaller apertures will undoubtedly decrease the observed level of aero-optical distortions and will change the apparent correlation length of the underlying optical structure.

All these conclusions are based on experimental data taken at one supersonic Mach number only, so all high-Mach-number trends presented in this paper should be treated as preliminary. More measurements at different supersonic Mach numbers should be taken to better understand the optical degradation caused by supersonic boundary layers.

### Acknowledgments

This work was partially funded by the U.S. Air Force Office of Scientific Research grant FA9550-09-1-0449. The U.S. Government is authorized to reproduce and distribute reprints for government purposes notwithstanding any copyright notation thereon. The authors would like to thank Danny Washburn for providing assistance in the Trisonic Tunnel measurements, especially the schlieren setup. They also thank the Director for Aeronautics Research Center, U.S. Air Force Academy, Thomas McLaughlin, for providing the opportunity to conduct the reported research.

### References

- [1] Gilbert, J., and Otten, L. J. (eds.), *Aero-Optical Phenomena*, Progress in Astronautics and Aeronautics, Vol. 80, AIAA, New York, 1982.
- [2] Jumper, E. J., and Fitzgerald, E. J., "Recent advances in aerooptics," *Progress in Aerospace Sciences*, Vol. 37, No. 3, 2001, pp. 299–339. doi:10.1016/S0376-0421(01)00008-2
- [3] Sutton, G. W., "Aero-Optical Foundations and Applications," *AIAA Journal*, Vol. 23, 1985, pp. 1525–1537. doi:10.2514/3.9120
- [4] Gordeyev, S., and Jumper, E., "Fluid Dynamics and Aero-Optics of Turrets," *Progress in Aerospace Sciences*, Vol. 46, 2010, pp. 388–400. doi:10.1016/j.paerosci.2010.06.001
- [5] Cress, J., Gordeyev, S., and Jumper, E., "Aero-Optical Measurements in a Heated, Subsonic, Turbulent Boundary Layer," 48th Aerospace Science Meeting and Exhibit, AIAA Paper 2010-0434, Orlando, FL, 4–7 Jan. 2010.
- [6] Cress, J. A., "Optical Distortions Caused by Coherent Structures in a Subsonic Compressible, Turbulent Boundary Layer," Ph.D. Thesis, University of Notre Dame, Notre Dame, IN, 2010.
- [7] Rose, W. C., "Measurements of Aerodynamic Parameters Affecting Optical Performance," U.S. Air Force Weapons Lab., TR AFWL-TR-78-191, May 1979.
- [8] Wyckham, C., and Smits, A., "Aero-Optic Distortion in Transonic and Hypersonic Turbulent Boundary Layers," *AIAA Journal*, Vol. 47, No. 9, 2009, pp. 2158–2168. doi:10.2514/1.41453
- [9] Stine, H. A., and Winovich, W., "Light Diffusion Through High-Speed Turbulent Boundary Layers," NACA RM A56B21, May 1956.
- [10] Liepmann, H. W., "Deflection and Diffusion of a Light Ray Passing Through a Boundary Layer," Douglas Aircraft Co., TR SM-14397, Santa Monica, CA, 16 May 1952.
- [11] Sutton, G. W., "Optical Imaging Through Aircraft Turbulent Boundary Layers," Progress in Astronautics and Aeronautics: Aero-Optical Phenomena, Vol. 80, edited by K. Gilbert, and L. J. Otten, AIAA, New York, 1982, pp. 15–39.
- [12] Yanta, W. J., Spring, W. C., III, Lafferty, J. F., Collier, A. S., Bell, R. L., Neal, D. R. et al., "Near- and Farfield Measurements of Aero-Optical Effects Due to Propagation Through Hypersonic Flows," 31st AIAA Plasmadynamics and Lasers Conference, AIAA Paper 2000-2357, Denver, CO, 19–22 June 2000.
- [13] Gordeyev, S., Hayden, T., and Jumper, E., "Aero-Optical and Flow Measurements over a Flat-Windowed Turret," *AIAA Journal*, Vol. 45, No. 2, 2007, pp. 347–357. doi:10.2514/1.24468
- [14] Wittich, D., Gordeyev, S., and Jumper, E., "Revised Scaling of Optical Distortions Caused by Compressible, Subsonic Turbulent Boundary Layers," 38th AIAA Plasmadynamics and Lasers Conference, AIAA Paper 2007-4009, Miami, FL, 25–28 June 2007.
- [15] Smits, A. J., and Dussauge, J.-P., *Turbulent Shear Layers in Supersonic Flow*, American Institute of Physics, Woodbury, NY, 1996.
- [16] Gordeyev, S., Jumper, E., Vukasinovic, B., Glezer, A., and Kibens, V., "Hybrid Flow Control of a Turret Wake, Part II: Aero-Optical Effects," 48th Aerospace Science Meeting and Exhibit, AIAA Paper 2010-0438, Orlando, FL, 4–7 Jan. 2010.
- [17] Bardina, J. E., Huang, P. G., and Coakley, T. J., "Turbulence Modeling Validation, Testing, and Development," NASA TM 110446, 1980.
- [18] Eckert, E. R. G., "Engineering Relations for Friction and Heat Transfer to Surfaces in High Velocity Flow," *Journal of the Aeronautical Sciences*, Vol. 22, No. 8, 1955, pp. 585–587.
- [19] Stratford, B. S., and Beaver, G. S., "The Calculation of the Compressible Turbulent Boundary layer in an Arbitrary Pressure Gradient—A Correlation of Certain Previous Methods," Aeronautical Research Council, Reports and Memoranda No. 3207, Ministry of Aviation, London, 1961.
- [20] Morkovin, M. V., "Effects of Compressibility on Turbulent Flows," *Mechanique de la Turbulence*, edited by Favre, A. J., Gordon and Breach, New York, 1962, pp. 367–380.
- [21] Sutton, G. W., "Effect of Turbulent Fluctuations in an Optically Active Fluid Medium," *AIAA Journal*, Vol. 7, No. 9, Sept. 1969, pp. 1737–1743. doi:10.2514/3.5384
- [22] Gilbert, K. G., "KC-135 Aero-Optical Boundary- Layer/Shear-Layer Experiments," *Aero-Optical Phenomena*, Progress in Astronautics and Aeronautics, Vol. 80, edited by K. G. Gilbert, and L. J. Otten, AIAA, New York, 1982, pp. 306–324.
- [23] Rose, W. C., and Johnson, E. A., "Unsteady Density and Velocity Measurements in the 6 × 6 ft Wind Tunnel," *Aero-Optical Phenomena*, Progress in Astronautics and Aeronautics, Vol. 80, edited by K. G. Gilbert, and L. J. Otten, AIAA, New York, 1982, pp. 218–232.

M. Glauser  
Associate Editor